DOI: 10.1002/ejic.200900425

Lanthanum Phosphite Microspheres: Hydrothermal Synthesis, Ab Initio Structure Determination, Morphology and Photoluminescence of $La(HO)(HPO_3)$

Ding-Bang Xiong,[a] Yu-Feng Zhao,[b] Lubomir D. Gulay,[c] and Jing-Tai Zhao*[a]

Keywords: Lanthanum phosphite / Ab initio calculations / Microspheres / Self-assembly / Structure elucidation / Luminescence

Lanthanum phosphite microspheres with diameters of 80–100 μm were obtained under hydrothermal conditions by using lanthanum oxalate as precursor. The surfaces of these spherules consist of well-orientated submicron-sized rods with typical diameters of 300 nm and lengths of 6 μm. The possible mechanism of formation of this morphology was suggested. The product is a new phase, and its crystal structure was determined by ab initio methods from high-resolution conventional X-ray powder diffraction analysis. Chains consisting of face-sharing LaO_9 polyhedra were observed; these chains form three-dimensional compact frameworks by sharing vertexes in the *ab* plane and edges along the *c* axis. The sample doped with Ce^{3+} showed an intensive broad emission band with a maximum around 364 nm under UV excitation.

Introduction

As an important category of functional materials, lanthanide phosphates are broadly used in the production of luminescent[1] and nonlinear optical materials,[2] scintillators,[3] biological labels,[4] photon up-conversion materials,[5] fibre coating materials[6] and so on. New compounds with various structures are expected to meet the requirements of emerging materials. $[PO_4]^{3-}$ is a tetrahedral anionic group, and phosphates can adopt structures with a great variety of connection patterns of anionic groups.[7] The phosphite ion $[HPO_3]^{2-}$ is a pseudo-tetrahedron with only three vertexes that are available for sharing by other polyhedra, unlike the four in the $[PO_4]^{3-}$ tetrahedron. This feature is expected to give rise to structures differing from four-connected polyhedron compounds.[7]

In contrast to the large number of transition metal phosphites and phosphates, reports on rare earth phosphites are rare.[8–19] We can summarize the structural features of these limited number of lanthanide phosphites in three points. Firstly, according to the connectivity of LnO_n (Ln = lanthanide) polyhedra, they can be sorted into two types of compounds, namely those containing chains or layers, and the layer type can also be decomposed into subunits of chains topologically. Secondly, the 3D LnO_n polyhedra framework is absent in all reported lanthanide phosphites except for the example of $La_2(HPO_3)_3$, in which six-membered LaO_9 polyhedra channels align along the *a* axis.[16] Thirdly, face-sharing LnO_n polyhedra are rarely observed.[18] Limited investigations on the properties of some lanthanide phosphites have been reported,[18,19] and the results showed that further research is necessary.

As a result of our ongoing investigations on structures and properties of lanthanide phosphites,[18,19] we report herein the growth of lanthanum phosphite microspheres, $La(HO)(HPO_3)$, prepared by a hydrothermal process with lanthanum oxalate as precursor. The X-ray powder diffraction (XRPD) pattern showed that the product has a new structure type, and its structure was solved by the ab initio structure determination method from conventional XRPD. The morphologies of these microspheres were described, and their possible formation mechanisms were also phenomenologically presented.

[a] The State Key Laboratory of High Performance Ceramics and Superfine Microstructure, Shanghai Institute of Ceramics, Chinese Academy of Sciences,
Shanghai 200050, P. R. China
Fax: +86-21-52413122
E-mail: jtzhao@mail.sic.ac.cn
[b] Nanyang Technological University, School of Materials & Engineering,
639798 Singapore
[c] Department of Ecology and Protection of Environment, Volyn National University,
Voli Avenue 13, Lutsk 43009, Ukraine

Supporting information for this article is available on the WWW under http://dx.doi.org/10.1002/ejic.200900425.

Results and Discussion

Ab Initio Structure Determination

X-ray diffraction patterns (Figure 1) were recorded by using a Rigaku D/max 2550V diffractometer with Cu-K_α

radiation of wavelength 1.5418 Å. Careful evaluation of the peak positions was carried out with a program available in the PC software WinXpow. No known matched phase was found, and indexing of the observed data led to the figure of merit FOM_{20} = 33.6 for the cell parameters a = 7.4856 Å, b = 5.1896 Å and c = 9.2738 Å. The crystal system was assigned as orthorhombic with systematic absences: *0kl*: $k + l = 2n$; *hk0*: $h = 2n$; *h00*: $h = 2n$; *0k0*: $k = 2n$; *00l*: $l = 2n$.

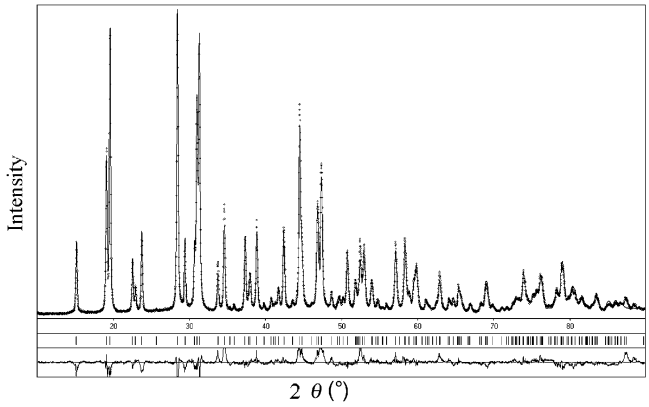

Figure 1. The experimental and calculated diffractograms for 2θ values ranging from 10° to 90° and the corresponding difference diagram for La(OH)(HPO$_3$).

The contents of the compounds were determined by energy dispersive spectroscopy (EDS), and no impurities of elements heavier than nitrogen were found except for trace amounts of sodium. The atomic percentages of La, P and O are 16.66%, 15.16% and 64.55%, respectively, and the corresponding molar ratio is La/P/O ≈ 1:1:4. In the starting materials, H_3PO_3 was used as phosphor source, and the presence of P–H linkages in the products was also confirmed by infrared spectroscopy, exhibiting strong and sharp peaks for υ(HP) at 2414 cm^{-1} and δ(HP) at 1041 cm^{-1}. Thus the species of $[La^{+3}O^{-2}(HPO_3)^{-2}]^-$ was deduced, and the final formula was assumed to be La(HO)(HPO$_3$) on the basis of valence balance, which agrees with the refinement results.

According to the cell dimensions and systematic absences, the possible space groups are *Pnma* and *Pna*2$_1$; the former is centrosymmetric and the latter is noncentrosymmetric. Because there were only two possible space groups, no other measurements such as second harmonic generation were carried out to confirm the space group, and *Pnma* was first chosen for its higher symmetry. After the structure was solved with space group *Pnma*, symmetries among the unique atoms were carefully checked, and the choice was finally confirmed.

Ab initio structure determination was performed by means of the Windows version of the Crystal Structure Determination program package (WinCSD).[20] The structural model obtained by direct methods in the space group *Pnma* was refined by using the full-profile mode (R_P = 18.16%, R_I = 16.18%). All non-hydrogen atoms, one La site, one P site and three O sites were obtained directly and refined.

Table 1. Results of the crystal structure determination of La(OH)(HPO$_3$).[a]

Space group	*Pnma*
a (Å)	7.4702(3)
b (Å)	5.1778(2)
c (Å)	9.2527(3)
V (Å^3)	357.89(4)
Z	4
Calculated density (g/cm^3)	4.3403(5)
Radiation	Cu-K_α
Wavelength (Å)	1.54178
Diffractometer	Rigaku D/MAX
Mode of refinement	Full profile
Programme	WinCSD
Number of free parameters	19
2θ	89.34
R_I, R_p	0.1618, 0.1816
Goodness of fit	1.030
Scale factor	0.3579(1)

[a] Cell parameters listed here are the final refined results, which are slightly different from the results of the indexing procedure.

Table 2. Atomic coordinates and temperature factors for La(OH)(HPO$_3$).

Atoms	Position	x	y	z	U_{iso} (Å^2)
La	4c	0.9857(3)	1/4	0.67513(2)	0.00317
P	4c	0.1271(11)	3/4	0.9229(8)	0.00317
O1	4c	0.948(2)	1/4	0.4121(14)	0.00317
O2	8d	0.181(2)	0.519(2)	0.8501(9)	0.00317
O3	4c	0.328(2)	1/4	0.572(2)	0.00317

Table 3. List of calculated and observed intensities and d-spacing of selected reflections for La(OH)(HPO$_3$).[a]

hkl	d	$I_{calcd.}$	$I_{obsd.}$	*hkl*	d	$I_{calcd.}$	$I_{obsd.}$
101	5.81267	22.5	19.2	411	1.72603	17.7	20.9
002	4.62668	38.6	41.4	031	1.6968	8.3	8.9
011	4.51879	78.5	77.9	314	1.61077	28.8	29.8
102	3.93342	22.6	16.4	132	1.58059	12.7	12.4
111	3.86648	8.3	7.1	215	1.57929	22.7	21.9
200	3.73528	25	20.8	323	1.55127	11.4	11.7
112	3.13223	100	92.1	231	1.54488	11.1	11.8
210	3.02938	19.6	20.2	006	1.54223	6.8	7.5
202	2.90634	17	16.4	125	1.47592	17.6	17.2
211	2.87902	56.8	58.6	422	1.43951	7	5.8
103	2.851	97.1	89.9	206	1.4255	11.1	10
013	2.64996	14.1	15.4	134	1.36029	14.1	12.1
020	2.58911	24.4	33.1	332	1.35628	7	5.8
301	2.40463	21.6	23.6	040	1.29455	7.1	6.8
203	2.37837	5	4.6	017	1.28083	19.1	18.4
121	2.3651	9.1	10.2	035	1.26227	5.9	5.9
004	2.31334	22.6	27.8	431	1.25589	8.3	8.4
213	2.1613	6.2	7	226	1.24874	18.4	18.8
220	2.12791	25.3	29.9	514	1.21977	11.5	10.4
114	2.03248	75.2	81.2	217	1.21158	22.5	21
312	2.01918	15.6	17.8	235	1.19583	6.4	6.1
303	1.93756	26.5	30.6	523	1.19332	9.4	8.6
222	1.93324	13.8	16.1	406	1.18919	8.5	7.6
123	1.91669	52.3	62.1	143	1.17873	9.9	8.9
105	1.79637	24.6	24.5	008	1.15667	7.2	8.5
321	1.76194	8.9	9.9	341	1.13987	5	5
015	1.74272	19.8	25.3	118	1.11618	5.9	6.4
402	1.73186	5.4	6.5	208	1.10491	6.2	6.2

[a] Only reflections with relative intensity greater than 5 are listed.

Hydrogen atoms were not located during the refinement but added according to the geometry of $(HPO_3)^{2-}$ and valence balance when describing the structure. Additional information on data collection and structure refinement and atomic parameters at the final stage of of crystal structure refinement are presented in Tables 1 and 2, respectively. The observed and calculated intensities are given in Table 3.

Structure Description and Evaluation

There are five crystallographically distinct non-hydrogen atoms in the title compound: one lanthanum, one phosphor in the $(HPO_3)^{2-}$ tetrahedral anionic group and three oxygen atoms. The La atom is ninefold coordinated by oxygen atoms (Figure 2d): six of the oxygen atoms (O2 and O3) are linked by six $(HPO_3)^{2-}$ tetrahedral anionic groups and shared by two other La atoms at the same time, which results in two pairs of face-sharing LaO_9 polyhedra. The remaining three oxygen atoms (O1) are shared by four La atoms, two pairs of neighbouring edge-sharing LaO_9 polyhedra forming a "VVV" shaped branch on the surface of the centred polyhedron, where each O1 is connected by one H atom additionally. Each of the three oxygen atoms in the $(HPO_3)^{2-}$ tetrahedral anionic group (two O2 atoms and one O3 atom) is shared by a pair of face-sharing LaO_9 polyhedra. The La–O lengths range from 2.450(13) to 2.756(5) Å with an average of 2.650(11) Å, and the P–O3 length is 1.42(2) Å, and the P–O2 lengths are 1.429(11) Å. All bond lengths are in the normal ranges and are listed in Table 4.

As indicated by the above description, LaO_9 polyhedra connected in three ways, namely by vertex-, edge- and face-sharing, are found in the title compound. The face-sharing polyhedra form zigzag chains along the *a* axis, and these chains are connect to each other side by side through vertexes in the *ab* plane (Figure 2c). These planes are also linked by their edges and pile up along the *c* axis to form the most condensed 3D LaO_n polyhedra framework in lanthanide phosphites (Figure 2a). Phosphite groups are linked to the 3D LaO_9 polyhedra framework through vertexes, and no phosphite groups are connected to each other (Figure 2c).

Because of the short interaction distances between lanthanide ions, compounds containing face-sharing polyhedra are expected to show interesting properties such as magnetism and photoluminescence.[21,22] Face-sharing LnO_n polyhedra are rarely observed in lanthanide phosphites. The face-sharing LaO_9 polyhedra are present in $La(H_2O)_x(HPO_3)_3$ (x = 1, 2) as dimers,[18] while they extend to chains in the title compound here. Under the same hydrothermal conditions, Pr adopted the same structure type $La(H_2O)_2(HPO_3)_3$ and demonstrated antiferromagnetic behaviour.[18] Similarly, the chains of face-sharing LaO_9 polyhedra and the condensed framework in the title compound are expected to be observed in other lanthanide phosphites, at least some light lanthanides, and related investigations are in progress.

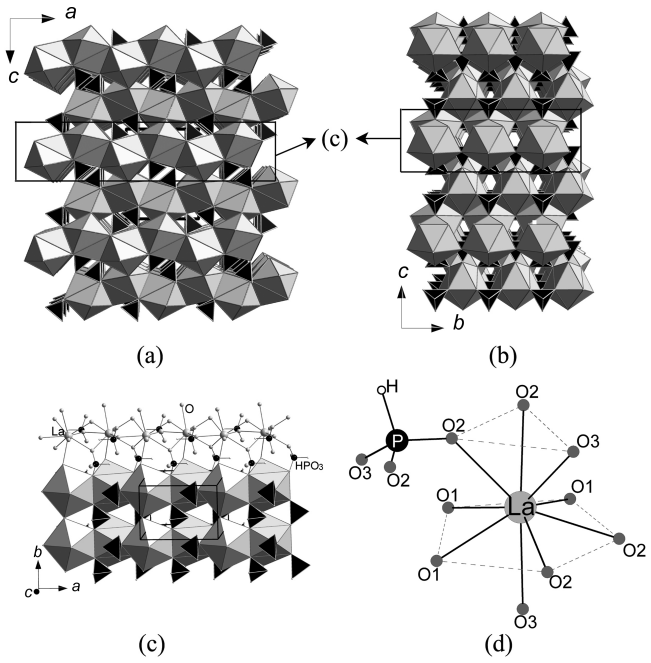

Figure 2. Crystal structure of La(HO)(HPO_3). (a) LaO_9 polyhedra layers (grey) piled up along the *c* axis by sharing edges, and phosphite anionic groups (black) located in the voids between them; (b) view of the structure along the *a* axis; (c) the parts indicated in (a) and (b) by rectangles consist of face-sharing LaO_9 polyhedra chains connected to each other side by side through vertexes; (d) coordination environment of La and P atoms.

Table 4. Selected bond lengths (Å) for La(OH)(HPO_3).

La–O1	2.450(13)	P–O3	1.42(2)
La–O2 (× 2)	2.588(10)	P–O2 (× 2)	1.429(11)
La–O3	2.622(15)		
La–O2 (× 2)	2.679(12)		
La–O3	2.73(2)		
La–O1 (× 2)	2.756(5)		

Spherical Microstructures

Spherical morphology is an interesting topic in crystal growth, and it was observed in various reported systems of both organic and inorganic compounds.[23] At the same time, various mechanisms were proposed. Sahni et al.[23a] suggested that crystallites were constrained to remain in a spherule in order to occupy a minimum volume. Keith and Padden[24] attributed spherical crystallization to high viscosity and the presence of impurities. According to Bolotov and Muravev,[25] spherules grow from a single crystal nucleus, they are drawn out in a direction perpendicular to the *c* axis lying in the plane of the crystal, and the circular shape is a result of surface tension forces acting on the different faces. Kniep et al.[26] explained the role of the intrinsic electrical fields in the formation of some spherical materials.

Here, crystallization of mixtures of lanthanum oxalate with H_3PO_3 produced well-defined La(HO)(HPO_3) spher-

ules 80–100 μm in diameter (Figure 3a). As shown in Figures 3a and 3b, we can see clearly the junctures (indicated by black lines) where two hemispheres are connected to each other. Similar aggregates were also observed at the later stages during the growth of anisotropic fluorapatite spheres reported by Kniep et al.[26] and of $BaCO_3$ reported by Yu et al.[27] According to these studies, the formation process of the spheres begins with elongated seeds, then progressive stages of fractal branching follow, which lead to dumbbell-shaped aggregates. The shapes are completed by successive and self-similar upgrowths to give notched spheres. In our case, two features suggest that the microspheres have crusts on their surface. The first one is the difference in orientation between the textures of the interior sphere and the exterior crust. In Figure 3f, the enlarged electron probe microanalyzer (EPMA) image shows that the crusts of the microspheres were built from small and elongated spindly building blocks with a typical diameter of 300 nm and length of 6 μm, which apparently adopted a well-orientated appearance. The cut sections inside the spheres reveal a texture of radial growth starting from the centre of the spherules (Figure 3c). The radial direction is different from the orientation of those well-orientated submicron-sized rods in the crust. The second feature is that the stability of the interface between the interior spheres and exterior crust decreases under physical treatment, such as heating.[26]

The $La(HO)(HPO_3)$ phase transformed into $LaPO_4$ as confirmed by XRD (ICSD No. 31564) after it was calcined at 500°C for 5 h, while the spherical morphology remained intact (Figure 4a). From the EPMA micrographs, we can see that the alignment of nanorods is denser than that in $La(HO)(HPO_3)$. It is interesting to see that there are some concaves and cracks on the crust of the calcined phases in Figure 4b. This phenomenon implies the existence of an interface between the interior spheres and the exterior crust and shows that they can be separated by physical treatment. As shown in Figures 3d and 4b, the thickness of the crust is around 5 μm.

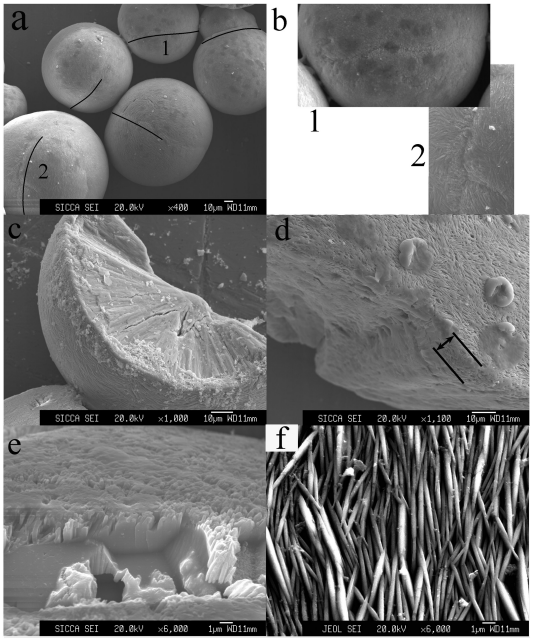

Figure 3. (a) Electron micrograph showing the spherical morphology of pure $La(HO)(HPO_3)$ (bar = 10 μm). The conjuncture tracks are highlighted by the black lines; (b) highlighted conjuncture tracks 1 and 2 in (a). (c) and (d) Electron micrographs of the half-spheres (bar = 10 μm): (c) illustrates the interior sections with radial growth, and (d) shows the cross section of the submicron-sized nanorods in the crust (arrow and lines indicate the thickness of the crust). (e) The commencement of the growth of submicron-sized nanorods on the surface and (f) electron micrograph illustrating a small region of the panel on the surface of as-grown microspheres in (a) at a higher magnification, which shows small, well-orientated rod-like crystals (bar = 1 μm).

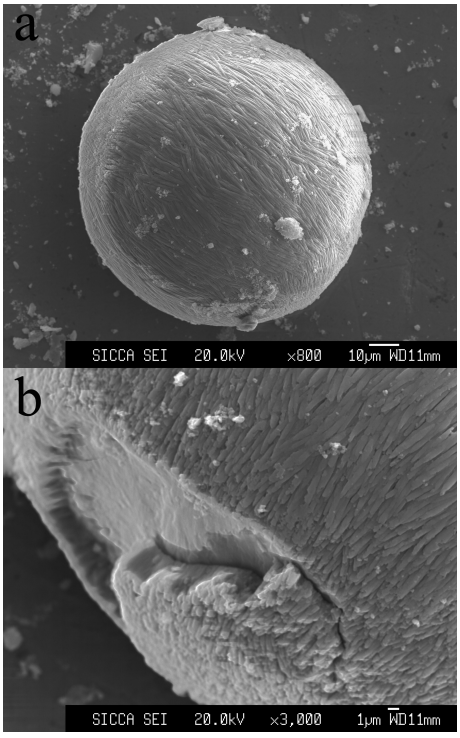

Figure 4. (a) The spherical $La(HO)(HPO_3)$ products transformed into $LaPO_4$ with the same morphology after being calcined at 500°C for 5 h; (b) electron micrograph showing the concave and crack on the crust of the calcined sphere, indicating the decreased stability of the interface between the core and crust as a result of heating.[26]

In this part, we will discuss the possible role of the lanthanum oxalate precursors in the formation of submicron-sized rods and then bring forward the possible mechanism for our case. Qian et al. prepared CdS, CdSe and CdTe nanorods and observed that the obtained samples adopted a rod-like shape only in bidentate solvents such as ethylenediamine and 1,6-diaminohexane.[28] Herein, oxalic acid is a bidentate ligand and reacts with La^{3+} to form stable lanthanum oxalate. At some relatively high temperature and high pressure under hydrothermal conditions, the complexes dissolve in water, and the stability of the complexes is expected to decrease. Then, phosphite anion groups coor-

dinate to the above complexes, and the coordinated ligands come apart gradually. In the processes of the formation of $La(HO)(HPO_3)$, the bidentate ligand oxalic acid could serve as a capping molecule and react with the anionic species during the nucleation and growth stages, leading to the formation of nanorods or elongated crystals. These nanorods or elongated crystals act as the seeds for the following mesoscale growth. On the basis of the observation of the surface or cross section of the as-grown microspheres described above, the formation of the interior spherules may be due to one of the following two possible mechanisms: (1) As suggested by Busch and Kniep,[26] with the growth of these nanorods, their ends could have branched and the formation of dumbbell intermediates started, and then the two ends of the dumbbells could have closed gradually; (2) alternatively, these tiny nanorods could have been constrained to remain in a spherule in order to occupy a minimum volume by accommodating themselves in a spherical space.[23b] As mentioned above, these interior spherules were covered by crusts composed of submicron-sized rods. Following one of the two possible processes above, the tips of the last generation of the interior spherules could have acted as nucleation centres for the growth of the next concentric crusts. In Figure 3e, we can see the commencement of the growth of the submicron-sized rods in the crust. Similarly, the shapes of the rods in the crust were controlled by the same possible mechanism in which oxalic acid molecules act as capping molecules.

Photoluminescence

Because of their fast decay time, Ce^{3+} doped inorganic materials are broadly used as scintillators for the detections of gamma-ray and high-energy particles.[29] In the course of ongoing investigations on the development of new scintillators in our group,[30] studies on the photoluminescence properties of $La(HO)(HPO_3)$ doped with Ce^{3+} under UV excitation were carried out. The emission and excitation spectra of $La(HO)(HPO_3):Ce^{3+}$(1.5%) at room temperature are presented in Figure 5. By monitoring the emission at 364 nm, the f–d excitation band of Ce^{3+} can be observed with peaks at 239, 262 and 284 nm in $La(HO)(HPO_3):Ce^{3+}$. The emission spectrum shows a broad peak centred at 364 nm. A Gauss fit to the spectrum with two peaks (the goodness of fit R = 99.54%) shows one main peak at 359 nm [FWHM (full width at half maximum) = 40 nm] and another peak at 386 nm (FWHM = 55 nm), corresponding to the $5d\rightarrow{}^2F_{5/2}$ (4f) and $5d\rightarrow{}^2F_{7/2}$ (4f) transitions, respectively. The F_J (J = 7/2, 5/2) energy gap of Ce^{3+} in the title compound is 1947 cm^{-1}, which is close to the F_J (J = 7/2, 5/2) energy gap of Ce^{3+} (2000 cm^{-1}) in most Ce^{3+} activated phosphors.[30e] When the peak in the emission spectrum of $La(HO)(HPO_3):Ce^{3+}$ is compared with that of Ce^{3+} doped $La_2(H_2O)(HPO_3)_3$ and $La_2(H_2O)_2(HPO_3)_3$,[18] the positions of the peaks shift from about 340 nm in the latter two to 364 nm in the former one. The difference between them can be explained as follows: The 5d excited state of rare earth ions is strongly influenced by the local vibrational mode, and the vibrational energy levels relate to the distance between the central rare earth ion and the coordinated oxygen atoms. The number of coordinated oxygen atoms in $La(HO)(HPO_3)$ and $La_2(H_2O)(HPO_3)_3$ and $La_2(H_2O)_2(HPO_3)_3$ are 9, 8 and 9, 9 and 9, and the average distances d(La–O) are 2.650(11), 2.548(3) and 2.573(3), 2.578(5) and 2.591(5) Å, respectively. The La–O bonds in $La(HO)(HPO_3)$ are obviously longer than those in the latter two compounds; in turn, the configuration coordinate of 5d in $La(HO)(HPO_3)$ is broader. As a result, the emission peaks in $La(HO)(HPO_3)$ shift toward long wavelengths. All results show the influence of the local environment of the dopant ions on the positions of their emission peaks in these compounds, and doping or co-doping with other lanthanide ions are worthy of investigation.

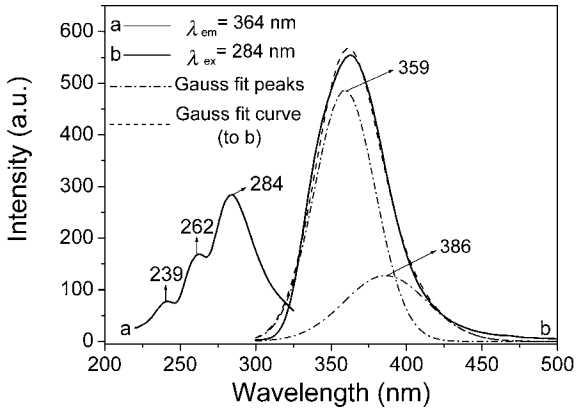

Figure 5. The UV excitation (a) and emission (b) spectra of $La(HO)(HPO_3):Ce^{3+}$.

Conclusions

A new compound, $La(HO)(HPO_3)$, was obtained by hydrothermal treatment with lanthanum oxalate as precursor. The structure of this new compound was solved by ab initio methods from X-ray powder diffraction data. The vertex-, edge- and face-sharing LaO_9 polyhedra form a compact 3D framework, and phosphite groups share all their oxygen vertexes with LaO_9 polyhedra. The products crystallize in microspheres with crusts made of well-orientated submicron-sized rods. After they were calcined at 500°C for 5 h, these spherical $La(HO)(HPO_3)$ products can transform into $LaPO_4$; however, the morphology remains intact, and the crust can be separated from the interior spheres partially. The title compound doped with Ce^{3+} showed an intensive broad emission band with a maximum around 364 nm under UV excitation.

Experimental Section

Synthesis: Inorganic chemicals and oxalic acid were reagent grade and used without further purification. Lanthanum chloride stock solutions of 0.5 M were prepared by dissolving the corresponding metal oxide in hydrochloric acid at elevated temperature, and the

stock solution of 0.8 M oxalic acid was prepared by dissolving oxalic acid (1.44 g) in deionized water (20mL).

In a typical procedure for the preparation of the products, H_3PO_3 (0.82 g, 0.01 mol) was dissolved in deionized water (10mL). Lanthanum oxalate complexes were prepared by mixing together $LaCl_3$ (20 mL, 0.5 M) and oxalic acid (20 mL, 0.8 M) stock solutions. The precipitate of lanthanum oxalate was filtered and washed with distilled water, then added into a solution of H_3PO_3 and the initial pH of the solution was adjusted by NaOH to about 12 while stirring. The mixture was stirred for 1 h at room temperature with the addition of NaCl as mineralizer. After that, the mixture was transferred into a Teflon-lined stainless steel autoclave with a volume of 20mL and heated for 5 d at 180°C under autogenous pressure. After cooling, the solids were washed with distilled water, and once with anhydrous ethanol, and dried overnight at 70°C in air before further characterization. In order to get the $LaPO_4$, the $La(HO)(HPO_3)$ phase was calcined for 5 h at 500°C in muffle furnace, and the structure was confirmed by XRPD.

Characterization: The morphologies of the grown crystals were examined by an electron probe microanalyzer (EPMA, model JSM-6700F, JEOL, Japan). Energy dispersive spectroscopy (EDS) data were recorded with an INCA analyzer having an attachment of an EPMA (model $8705QH_2$, Shimadzu, Japan) for carrying out the elemental analysis of the grown crystals. The IR spectrum was collected with a Digilab-FTS-80 spectrophotometer by using pressed KBr pellets of the samples. UV luminescence spectra were recorded with a Shimadyn RF-5301 spectrofluorophotometer at room temperature, and a 450 W xenon lamp was used as an excitation source.

Supporting Information (see footnote on the first page of this article): EDS and FTIR spectra for $La(HO)(HPO_3)$, and XRPD spectrum for $LaPO_4$.

Acknowledgments

The authors thank Prof. Guang-Lie Lv from Zhejiang University (Hangzhou, China) for the collection of XRPD data. This work was supported by the Key Project of the National Natural Science Foundation of China (50332050), the Hundred Talents Program of the Chinese Academy of Sciences and by funds for Young Leading Researchers from the Shanghai municipal government.

[1] K. Riwotzki, H. Meyssamy, H. Schnablegger, A. Kornowski, M. Haase, *Angew. Chem. Int. Ed.* **2001**, *40*, 573–576.
[2] J. J. Carvajal, I. Parreu, R. Sol, X. Solans, F. Daz, M. Aguil, *Chem. Mater.* **2005**, *17*, 6746–6754.
[3] L. A. Boatner, L. A. Keefer, J. M. Farmer, D. Wisniewski, A. Wojtowica, *Proc. SPIE* **2004**, *5540*, 73–87.
[4] C. R. Patra, R. Bhattacharya, S. Patra, S. Basu, P. Mukherjee, D. Mukhopadhyay, *Clin. Chem.* **2007**, *53*, 2029–2031.
[5] S. Heer, O. Lehmann, M. Haase, H. U. Güdel, *Angew. Chem. Int. Ed.* **2003**, *42*, 3179–3182.
[6] E. E. Boakyew, P. Mogilevsky, R. S. Hay, G. E. Fair, *J. Am. Ceram. Soc.* **2008**, *91*, 3841–3849.
[7] S. Natarajan, S. Mandal, *Angew. Chem. Int. Ed.* **2008**, *47*, 4798–4828.
[8] Y. Zhang, H. Hu, A. Clearfield, *Inorg. Chim. Acta* **1992**, *193*, 35–42.
[9] J. A. Seddon, A. R. W. Jackson, R. A. Kresinski, A. W. G. Platt, *J. Chem. Soc., Dalton Trans.* **1999**, 2189–2196.
[10] M. Loukili, J. Durand, L. Cot, M. Rafiq, *Acta Crystallogr., Sect. C* **1988**, *44*, 6–8.
[11] M. Loukili, J. Durand, A. Larbot, L. Cot, M. Rafiq, *Acta Crystallogr., Sect. C* **1991**, *47*, 477–479.
[12] N. Tijani, J. Durand, L. Cot, *Acta Crystallogr., Sect. C* **1988**, *44*, 2048–2050.
[13] J. D. Foulon, N. Tijani, J. Durand, M. Rafiq, L. Cot, *Acta Crystallogr., Sect. C* **1993**, *49*, 849–851.
[14] J. D. Foulon, N. Tijani, J. Durand, M. Rafiq, L. Cot, *Acta Crystallogr., Sect. C* **1993**, *49*, 1–4.
[15] J. D. Foulon, J. Durand, L. Cot, N. Tijani, M. Rafiq, *Acta Crystallogr., Sect. C* **1995**, *51*, 348–350.
[16] B. Ewald, Yu. Prots, R. Kniep, *Z. Kristallogr. – New Cryst. Struct.* **2005**, *220*, 533–534.
[17] B. S. Zakharova, A. B. Ilyukhin, N. N. Chudinova, *Zh. Neorg. Khim. (Russ. J. Inorg. Chem.)* **2003**, *48*, 2004–2007.
[18] D. B. Xiong, M. R. Li, W. Liu, H. H. Chen, X. X. Yang, J. T. Zhao, *J. Solid State Chem.* **2006**, *179*, 2571–2577.
[19] D. B. Xiong, Z. J. Zhang, L. D. Gulay, M. B. Tang, H. H. Chen, X. X. Yang, J. T. Zhao, *Inorg. Chim. Acta* **2009**, *362*, 3013–3018.
[20] L. G. Akselrud, Yu. Grin, V. K. Pecharsky, P. Zavalij, *WinCSD*, version 10.2005, **2005**.
[21] Y. L. Huang, M. Y. Huang, T. H. Chan, B. C. Chang, K. H. Lii, *Chem. Mater.* **2007**, *19*, 3232–3237.
[22] F. Millange, C. Serre, J. Marrot, N. Gardant, F. Pellé, G. Férey, *J. Mater. Chem.* **2004**, *14*, 642–645.
[23] a) V. Hangloo, S. Pandita, K. K. Bamzai, P. N. Kotru, N. Sahni, *Cryst. Growth Des.* **2003**, *3*, 753–759 and related references; b) V. Hangloo, S. Pandita, K. K. Bamzai, P. N. Kotru, N. Sahni, *J. Mater. Sci.* **2004**, *39*, 1743–1749; c) S. Škapin, I. Sondi, *Cryst. Growth Des.* **2005**, *5*, 1933–1938.
[24] H. D. Keith, F. J. Padden, *J. Appl. Phys.* **1963**, *34*, 2409–2421.
[25] I. E. Bolotov, E. W. Muravev in *Growth and Imperfections of Metallic Crystals* (Ed.: D. E. Ovsienko), Consultants Bureau, New York, **1968**, p. 76.
[26] a) S. Busch, U. Schwarz, R. Kniep, *Adv. Funct. Mater.* **2003**, *13*, 189–198; b) S. Busch, H. Dolhaine, A. DuChesne, S. Heinz, O. Hochrein, F. Laeri, O. Podebrad, U. Vietze, T. Weiland, R. Kniep, *Eur. J. Inorg. Chem.* **1999**, 1643–1653.
[27] S. H. Yu, C. Helmut, A. W. Xu, W. F. Dong, *Cryst. Growth Des.* **2004**, *4*, 33–37.
[28] Y. D. Li, H. W. Liao, Y. Ding, Y. T. Qian, L. Yang, G. E. Zhou, *Chem. Mater.* **1998**, *10*, 2301–2303.
[29] J. C. van't Spijker, *Luminescence & Scintillation of Ce^{3+} Doped Inorganic Materials for Gamma-Ray Detection*, Thesis, Delft University Press, **1999**.
[30] a) J. T. Zhao, C. J. Duan, "New Potential Scintillation Materials in Borophosphate Systems", in *Inorganic Chemistry in Focus III* (Eds.: G. Meyer, D. Naumann, L. Wesemann), Wiley-VCH, **2006**, pp. 305–324; b) C. J. Duan, X. Y. Wu, W. F. Li, H. H. Chen, X. Q. Feng, J. T. Zhao, *Appl. Phys. Lett.* **2005**, *87*, 201917–1-201917–3; c) M. R. Li, W. Liu, H. H. Chen, X. X. Yang, Z. B. Wei, D. H. Cao, M. Gu, J. T. Zhao, *Eur. J. Inorg. Chem.* **2005**, 4693–4696; d) J. L. Yuan, X. J. Wang, D. B. Xiong, C. J. Duan, J. T. Zhao, Y. B. Fu, G. B. Zhang, C. S. Shi, *J. Lumin.* **2007**, *126*, 130–134; e) Z. J. Zhang, J. L. Yuan, C. J. Duan, D. B. Xiong, H. H. Chen, J. T. Zhao, G. B. Zhang, C. S. Shi, *J. Appl. Phys.* **2007**, *102*, 093514-1–093514-7.

Received: May 10, 2009
Published Online: September 4, 2009

